# ATR-FTIR to distinguish Holocene fumier facies: a perspective from bone diagenesis at El Mirador cave (Sierra de Atapuerca, Spain)

Del Valle, H.; Cáceres, I.; Tornero, C.; Burguet-Coca, A.; Moclán, A.; Vergès, J.M.

Journal of Archaeological Science 141 (2022) 105582

Contents lists available at ScienceDirect

Journal of Archaeological Science

journal homepage: www.elsevier.com/locate/jas

# ATR-FTIR to distinguish Holocene *fumier* facies. A perspective from bone diagenesis at El Mirador cave (Sierra de Atapuerca, Spain)

Héctor Del Valle [a,b,*], Isabel Cáceres [b,a], Carlos Tornero [c,a,b], Aitor Burguet-Coca [d,a,b], Abel Moclán [e,f,g], Josep Maria Vergès [a,b]

[a] Institut Català de Paleoecologia Humana i Evolució Social (IPHES-CERCA), Zona Educacional 4, Campus Sescelades URV (Edifici W3), 43007, Tarragona, Spain
[b] Universitat Rovira i Virgili, Departament d'Història i Història de l'Art, Avinguda de Catalunya 35, 43002, Tarragona, Spain
[c] Department of Prehistory, Autonomous University of Barcelona (UAB), Edifici B, 08193, Bellaterra (Cerdanyola del Vallès), Spain
[d] Department of Archaeological Sciences, Faculty of Archaeology, Leiden University, Einsteinweg 2, 2333CC, Leiden, The Netherlands
[e] Centro Nacional de Investigación sobre la Evolución Humana (CENIEH), Paseo Sierra de Atapuerca, 3, 09002, Burgos, Spain
[f] Escuela Interuniversitaria de Posgrado en Evolución Humana, Universidad de Burgos, Don Juan de Austria 1, 09001, Burgos, Spain
[g] Institute of Evolution in Africa (IDEA), University of Alcalá de Henares, Covarrubias 36, 28010, Madrid, Spain

ARTICLE INFO

*Keywords:*
Diagenetic parameters
Archaeological bones
Bioapatite
Facies
ATR-FTIR
Holocene

ABSTRACT

Long and complex sequences of intentional organic rich sediments accumulation known as *fumiers* can often be found in many caves and rock shelters used for herding activities since the Neolithic to current times in the Mediterranean basin. These are mainly composed of burnt animal dung and vegetal remains and are commonly interpreted as the result of livestock domestic occupations and stabling activities. The repetitive and systematic burning processes that occurred for cleaning these spaces provide different layers with different archaeosedimentary features (facies). *Fumier* facies imply different pre-burial conditions that may influence bone diagenetic processes. In this work, we study the changes occurring in mineral and organic components of bones included in different facies (reelaborated, burned, unburned) in El Mirador cave *fumier* using Attenuated Total Reflectance Fourier Transform Infrared spectroscopy (ATR-FTIR). We have carried out an analysis of 47 bone remains from four different facies [*a*, *r(m)*, *tf* and *v*] from archaeological levels dated from the second half of the 5th until the first half of the 2nd millennia cal B.C. We have used a total of 13 parameters through ATR-FTIR to discriminate facies differences through PCA and Machine Learning techniques. The results show differences in crystallinity, organic, and carbonates content between bone remains recovered from *fumier* facies. Our results demonstrate that burial environments that occur on *fumier* deposits affect bone components in different ways. Therefore, *fumier* facies can be differentiated from each other through the diagenetic parameters provided by bone assemblage, distinguishing those well preserved and, therefore, eligible for other types of analyses (isotopes, proteomics, lipids, etc.). Furthermore, Machine Learning can classify the facies through carbonates indices API, C/C, and BPI. This study is an important step towards understanding the taphonomic processes (formation and reelaboration) that occur in *fumier* sequence as a result of the multiple livestock activities developed in caves and rock shelters.

## 1. Introduction

Bone diagenesis refers to the preservation or destruction of the components of bone. Bone is a composite material with a complex structure that can be divided into organic components (mainly type-I collagen) and mineral components consisting of bioapatite (Weiner and Wagner, 1998; Nielsen-Marsh and Hedges, 2000; Collins et al., 2002; Dal Sasso et al., 2016; Kendall et al., 2018). The mineral phase of fresh bone is described as a poorly crystalline non-stoichiometric carbonate hydroxylapatite (Lebon et al., 2008). According to Pasteris et al. (2008, 2014) their mineralogical phase is defined as a combined hydrated-hydroxylated calcium phosphate, whose formula is summarized as $Ca_{10-x}[(PO_4)_{6-x}(CO_3)_x](OH)_{2-x}{\cdot}nH_2O$.

The study of bone diagenesis for a specific site is used to understand

* Corresponding author. Universitat Rovira i Virgili, Departament d'Història i Història de l'Art, Avinguda de Catalunya 35, 43002 Tarragona, Spain.
*E-mail addresses:* hectorvalleblanco@gmail.com (H. Del Valle), icaceres@iphes.cat, isabel.caceres@urv.cat (I. Cáceres), ctornero@iphes.cat (C. Tornero), aitorburguetcoca@gmail.com (A. Burguet-Coca), abel.moclan@cenieh.es (A. Moclán), jmverges@iphes.cat (J.M. Vergès).

https://doi.org/10.1016/j.jas.2022.105582
Received 23 February 2021; Received in revised form 26 January 2022; Accepted 4 March 2022
Available online 11 March 2022

how these taphonomic processes have altered bones and teeth remains. Therefore, the study of diagenetic modification helps to get the reliability of recovered information for isotope analysis, dating, and proteomics (Weiner, 2010; Dal Sasso et al., 2014). During Fossildiagenesis, the remains are in the transition stage from the biosphere to the lithosphere. Many processes take place when the deterioration of bones and teeth occurs. Each context can present different conditions for its preservation resulting in a specific taphosystem (Fernández-López, 1991, 2006; Domínguez-Rodrigo et al., 2011).

While bone diagenesis in Holocene sites is widespread, its study in shepherds' caves is not so frequent. From diagenetic parameters, we can quickly find well-preserved bone remains as well as understand which are the most aggressive burial environments (Smith et al., 2007). The control of diagenetic parameters is important to obtain a good resolution for biomolecular information, but it is also important to understand cultural and taphonomic processes such as boiled and cooked bones (Botella, 2000; Roberts et al., 2002; Bosch et al., 2011).

The use of caves during recent Prehistory responds to a wide variety of cultural activities, whose result at the archaeological level translates into a great difficulty of interpretation. One of the main interpreted activities is livestock. These activities trigger the formation of a sequence composed of burned and unburned episodes organized in well-bedded layers (Friesem, 2016). The resulting product is named *fumier* (Brochier, 1991; Brochier et al., 1992, 2002; Angelucci et al., 2009; Oms

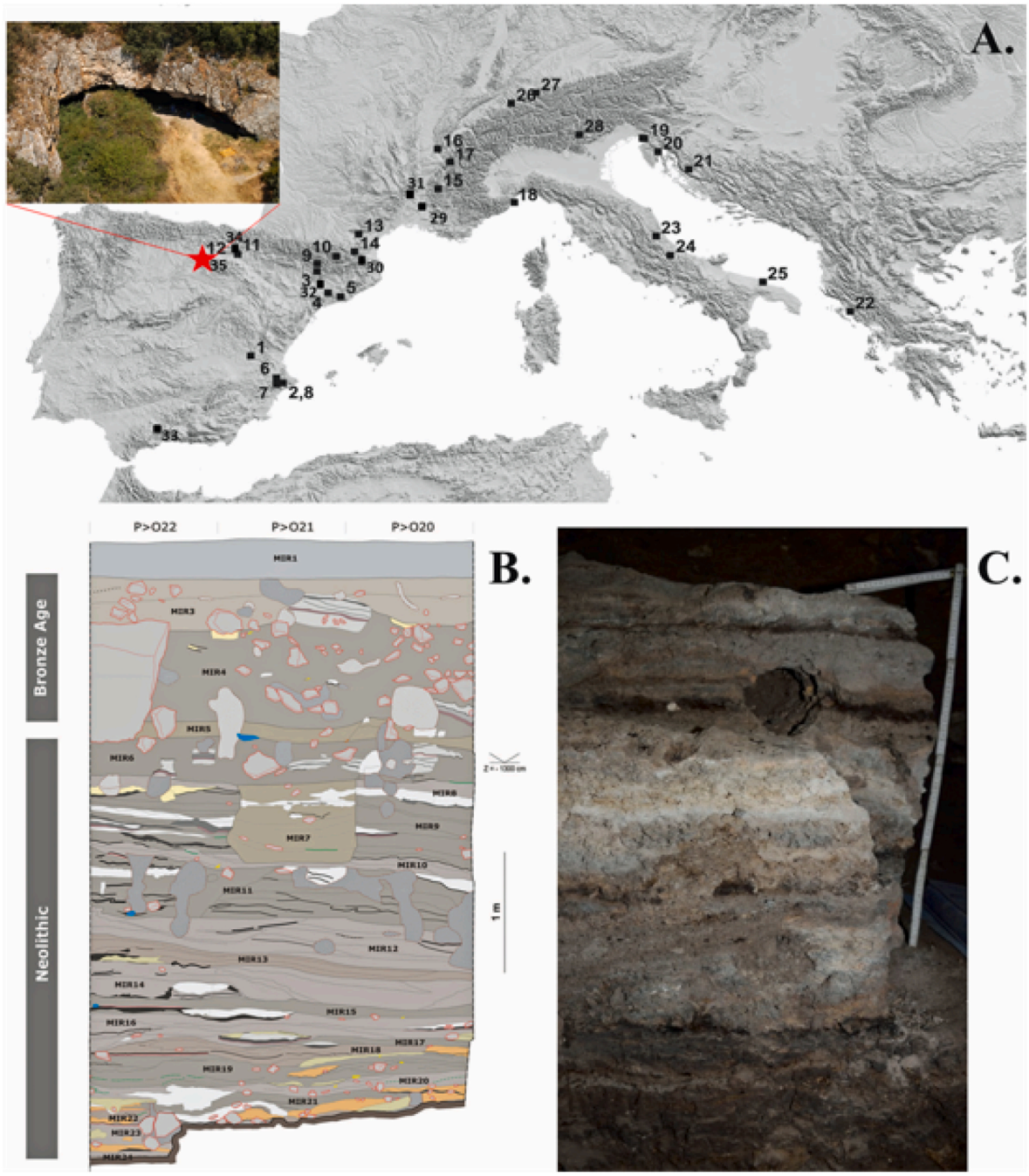


**Fig. 1. A)** Location of several *fumier* sites in the Mediterranean basin, modified from Angelucci et al. (2009). Red star, El Mirador cave. The different numbers for each site are specified in supplementary files, Table S11. **B)** Stratigraphy of the Holocene sequence from El Mirador cave; modified from Angelucci et al. (2009). **C)** View of the stratigraphic sequence with different facies from sector 100. (For interpretation of the references to colour in this figure legend, the reader is referred to the Web version of this article.)

et al., 2013; Polo et al., 2016; Martin-Rodriguez and Vergès, 2016), which is the result of the compaction of each burning episode and is integrated by several facies. *Fumier* means manure in French and it is usually accompanied by plant remains used for livestock litters or feeding (Argant et al., 1991).

A *fumier* is mainly composed of domestic herbivore dung (Polo-Diaz, 2010) and plant remains (spherulites, phytoliths, pollen, charcoal, and seeds noted for their high presence) (Brochier et al., 1992; Miller, 1996; Cabanes et al., 2009; Shahack-Gross, 2011; Expósito and Burjachs, 2016; Euba et al., 2016; Rodríguez et al., 2016; Burguet-Coca et al., 2020) burned to clean and deworm spaces dedicated to the stabling of livestock. These remains are commonly considered a product of pastoral activities. Due to this highly organic nature, they are a complex record at the taphonomic level. Since they mainly come from the combustion of organic waste, there is a great variety of depositional dynamics responsible for the variability in sedimentary facies (Macphail et al., 1997; Goldberg and Macphail, 2006; Angelucci et al., 2009). The sedimentary features of *fumier* deposits are almost identical in all the sites that have been recorded (Angelucci et al., 2009; Brochier, 2002; Spengler, 2019; Burguet-Coca et al., 2020). The main differences within archaeological *fumiers* have been documented in terms of the preservation and the extension within caves and rock shelters. These variations could be the result of differences in the spatial organization of the sites. A remarkable example of this type of assemblage is El Mirador Cave (Vergès et al., 2016).

El Mirador cave is located in the southern part of the karstic complex of Sierra de Atapuerca (Burgos, Spain). Its stratigraphic sequence stretches from the Upper Palaeolithic and the Early Neolithic to the Bronze Age. For at least 4000 years, the cave was mainly used for two types of activities: funerary burial and livestock enclosure (Cáceres et al., 2007; Cabanes et al., 2009; Expósito and Burjachs, 2016; Vergès et al., 2016; Martín et al., 2016, 2021; Euba et al., 2016; Marginedas et al., 2020). Due to these livestock activities, the deposits described in the three surveys have been described as sequences of *fumiers* (Vergès et al., 2016) (Fig. 1).

These deposits usually show well preserved bone surfaces (Martín--Rodríguez, 2015; Martín-Rodríguez and Vergès, 2016; Martín et al., 2021). This good preservation has also been observed in experimental studies on compost heaps by Nicholson (1996, 1998). So far, no *fumier* deposits have been analysed from a bone diagenetic perspective. We think it would be advisable to carry out at least one analysis through FTIR tool. Previous works have shown that FTIR is a powerful tool to study sediments of a *fumier* and the formation processes involved (Cabanes et al., 2009; Shahack-Gross et al., 2003, 2011; Gur-Arieh et al., 2014; Burguet-Coca et al., 2020).

Modification of the mineral and biomolecular properties of bone can be investigated by infrared spectroscopy (i.e. Weiner and Bar-Yosef, 1990; Stiner et al., 1995; Nielsen-Marsh and Hedges, 2000; Trueman et al., 2008; Thompson et al., 2009; Paschalis et al., 2011; Hollund et al., 2013, Grunenwald et al., 2014; Lebon et al., 2016; Dal Sasso et al., 2016, 2018; Kontopoulos et al., 2018; Leskovar et al., 2020). Although the traditionally used method has been the KBr bone powder method, here we provide an approach to bone preservation through ATR-FTIR. Recent studies have shown that ATR-FTIR is more successful on archaeological bone analysis (Hollund et al., 2013; Beasley et al., 2014). This is because it requires minimal and quick preparation, and a low amount of sample. Furthermore, it is sensitive in investigating both the mineral and organic phase, which leads to a reduction of potential analytical errors. In addition, semi-quantitative analyses can be performed to understand molecular relationships in archaeological bones. Besides, traditionally used indices such as Am/P, IRSF, C/P, BPI, or API can be explored with methods such as Machine Learning (ML) to improve classification and pre-screening results among bone remains (Pal Chowdhury et al., 2021).

The purpose of this study is to use ATR-FTIR spectroscopy to investigate a bone assemblage from different soil conditions (facies) in the *fumier* from El Mirador cave. Our main objectives are the following: 1) to characterize and distinguish the facies through the molecular information from bone remains; 2) to identify the facies with the best preservation at the molecular level of bone remains; 3) and to evaluate the incidence of fire in each facies through bone remains and ATR-FTIR indices.

## 2. Materials and methods

### 2.1. Bone samples

A total of 47 bone remains have been analysed for this study (Table S1 and Figure S1). These archaeological bone samples were obtained from different facies (Table 1) and collected from the archaeological sectors 200 and 100 from El Mirador cave (Fig. 1): facies *a* from MIR105 level (n = 10), facies *v* from MIR108 level (n = 10) and from MIR205 level (n = 10), respectively named v100 and v200, facies *tf* from MIR107 level (n = 10), and facies *r(m)* from MIR107 level (n = 7) defined by Angelucci et al. (2009) (Table 1). The samples belong to Late Neolithic (n = 37) and Middle Bronze age (n = 10).

Before analytical ATR-FTIR measurements, potential modifications occurring on the bone surfaces due to thermoalteration were noted using a stereomicroscope Euromex between 20x and 60x under a strong light (60 W). On the one hand, for a burned bone characterization we have distinguished 5 stages based on coloration (Shipman et al., 1984; Stiner et al., 1995; Cáceres, 2002). Stage 0, when no burned alteration is observed. Stage 1, when the bone surface has small scattered brown dots. Stage 2, partially homogeneous brown colour over the entire surface. Stage 3, the bone is charred, and its coloration is black. Stage 4, grey coloration with occasional streaks of bluish tones. Stage 5, totally white, calcined. On the other hand, to identify boiled bones, we have attended to smoothness, light transparency, yellowish-cream colour, and oily surface (White, 1992; Botella et al., 2000; Pijoan et al., 2007; Cáceres et al., 2007).

### 2.2. ATR-FTIR spectroscopy

FTIR analysis was performed in ATR mode (Fig. 2) (Beasley et al., 2014). Each bone sample was processed following the methodology proposed by Kontopoulos et al. (2018) and Lebon et al. (2016). The spectra were collected on a Jasco FT/IR-6800 spectrometer with a resolution of 2 $cm^{-1}$ and 64 scans in the range 4000–370 $cm^{-1}$ at the SCiT URV (University of Rovira i Virgili's Scientific and Technical service, Tarragona, Spain). Around 2 mg of sample powder was pressed on the surface of a diamond crystal and run in triplicate with a 50-20 μm particle size (Kontopoulos et al., 2018). The anvil pressure on the ATR crystal was adjusted to obtain a 0.5 absorbance for the $\nu_3(PO_4^{3-})$ band around 1010 $cm^{-1}$ (Lebon et al., 2016). Spectra analysis was performed using Omnic 9.8 software (Thermo Scientific). Based on previous studies

**Table 1**
Sedimentary features of the lithofacies analysed in this work. Modified from Vergès et al. (2016).

| Name | Short description | |
|---|---|---|
| ***a*** | Reelaborated facies | Yellowish brown clayey silt, with few to common unsorted calcareous stones, common organic matter, high porosity; it contains common ash and scarce microcharcoal fragments dispersed in the matrix. |
| ***r(m)*** | burned facies | Light brown massive (sometimes granular) accumulations of ash, containing mm-sized fragments of charcoal and reddened sediment. r- is used for presence of reddening |
| ***tf*** | burned facies | Silt with abundant ash and varied colour, sometimes with platy structure and moderate cementation |
| ***v*** | unburned facies | 3 to 5 cm-thick layers of clayey loam, massive o with parallel lamination, with intercalations of orange layers with fibrous or granular structure containing recognizable digested bones and coprolites. |

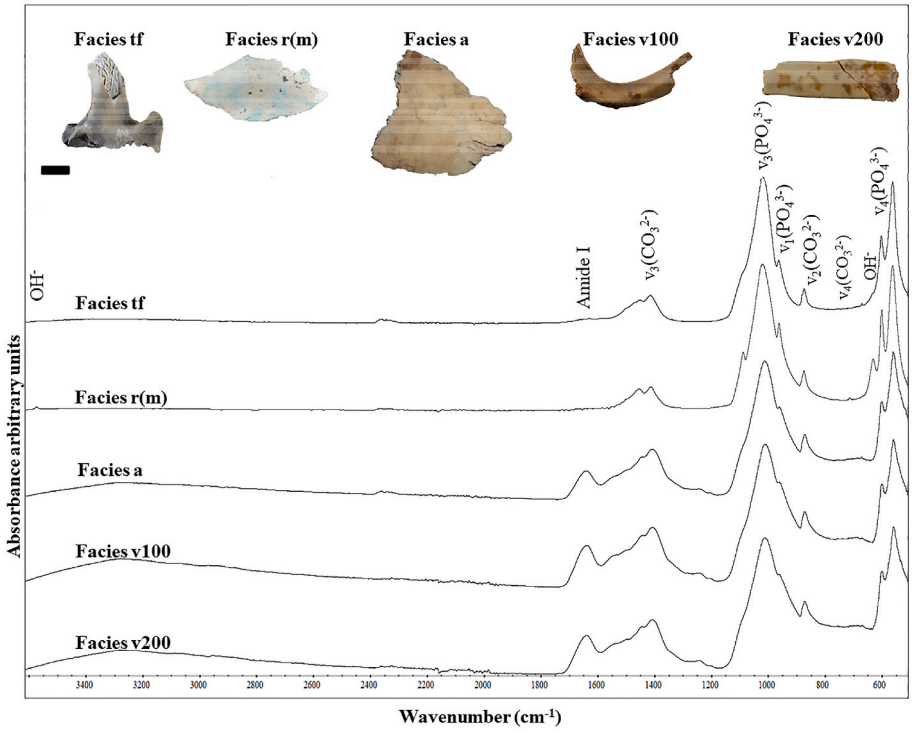


**Fig. 2.** Bone samples from each facies with the representative ATR-FTIR spectrum and assignments of the main bands.

that explore bone preservation, 13 indices were used in this study. Table 2 shows each index as well as the baseline correction used for each of them.

### 2.3. Collagen analysis

Collagen amount was estimated and pre-screening following Lebon et al. (2016) and using ATR-FTIR. Besides, collagen was extracted from 47 samples using the original acid-base-acid protocol proposed by Longin (1971) and modified in Bocherens et al. (1991). Sample preparation and collagen extractions were performed at the Biomolecular laboratory at the IPHES-CERCA (Catalan Institute of Human Paleoecology and Social Evolution, Tarragona, Spain). Bone samples were crushed to a powder of <0.7 mm grain size and ca. 300–350 mg of bone shards were soaked in 1M HCl for demineralization, in NaOH (0.125 M) to remove contaminants, rinsed with distilled water, and gelatinized with 0.01 M HCl at 100 °C for 17h. Finally, the solubilized collagen was filtered and freeze-dried for 48 h at the ICIQ (Institute of Chemical Research in Catalonia, Tarragona, Spain). Once was lyophilized, collagen extraction yield was calculated, *collagen yields (wt.%)= (mg of collagen extracted/mg of bone powder) × 100*.

### 2.4. Statistical analyses

Firstly, the results were expressed as the mean value ± standard deviation (Table S1). The previsualization of the indices was carried out through boxplot diagrams from the normalized spectra. The Shapiro-Wilk test was used to assess the normal distribution of the analysed variables. Bartlett's test was used to test homoscedasticity. Then we used a Welch's ANOVA test due to the Bartlett's test showing that the most part of the samples are non-homogeneous (p-values < 0.05). Considering that in few cases the variance of some samples is 0 (e.g. index Am/P of facies *r(m)*), Welch's ANOVA test has been applied only to the facies which allow a variance different to 0. In the specific case of the Cal/P variable, only facies *a* and *r(m)* show values higher than 0, so the comparison between them has been developed using a Wilcoxon rank-sum test. In order to improve all these analyses, we have used a non-parametric Kruskal-Wallis H test that compared all facies at the same time with each variable. Finally, we used Wilcoxon rank sum tests for pairwise comparison among groups. P-values < 0.05 were considered statistically significant (from Table S3 to Table S7). All these analyses were performed using the statistical software R version 3.5.1 (R Core Team, 2017). In order to observe the distribution of the variables and their contribution, a principal component analysis (PCA) was performed. The principal components are linear combinations of original variables that maximize the explained variance. The greater the accumulation of variance in the first two or three components, the better the representation and the less distortion the result will have with respect to the original data. Thus, a PCA reveals correlations between samples, revealing the most important spectra regions related to groupings of samples. All analyses were carried out with the software R version 3.5.1 (R Core Team, 2017), and "MASS" (Venables and Ripley, 2002), "FactoMiner" (Lê et al., 2008), and "Factoextra" libraries (Kassambara and Ripley, 2020).

Further to the previous classification analysis, Machine Learning (ML) techniques were used to classify the different facies with higher accuracy. ML algorithms are more powerful than traditional Fisherian and Bayesian tests (Domínguez-Rodrigo, 2019). Besides that, ML methods showed fewer limitations than traditional approaches on sample distribution and size (Domínguez-Rodrigo, 2019). This type of statistical approach allows the classification and prediction of targeted categories within analytical samples through the use of a powerful system of data evaluation (Kuhn and Johnson, 2013). This analysis was performed using the "caret" library in R (Kuhn et al., 2020). In order to develop this study, we have included all codes as supplementary material.

These algorithms have been used in taphonomic studies to analyse different bioestratinomic problems, such as the morphology of the bone surface modifications (Courtenay et al., 2019; Domínguez-Rodrigo and Baquedano, 2018), bone breakage (Moclán et al., 2019, 2020), or skeletal profiles (Arriaza and Domínguez-Rodrigo, 2016; Egeland et al., 2018), obtaining very accurate classification values (~100%).

**Table 2**
Diagenetic parameters calculated through ATR-FTIR for each bone sample.

| Indices | Peaks ($cm^{-1}$) | Description | Vibrational mode | Baseline correction ($cm^{-1}$) | Reference |
|---|---|---|---|---|---|
| Am/P | 1640/ 1010 | Amide I to phosphate | Amide I C═O<br>$\nu_3(PO_4)$ | 1710–1590<br>1150–890 | Trueman et al. (2004)<br>Lebon et al. (2016) |
| IRSF | (560 + 600)/ 590 | Infrared splitting factor. relative measurement indicating crystallite size and order | $\nu_4(PO_4)$ | 660/640 470/420 | Weiner and Bar-Yosef (1990) |
| C/P | 1410/ 1010 | Carbonate to phosphate | $\nu_3(CO_3)$ B-type | 1590–1290 | Wright and Schwarcz (1996) |
| BPI | 1410/ 600 | Relative amount of B-type carbonate to phosphate | | | Snoeck et al. (2014)<br>Sponheimer and Lee-Thorp (1999) |
| API | 1540/ 600 | Relative amount of A-type carbonate to phosphate | $\nu_3(CO_3)$ A-type | 1200–1800 | Sponheimer and Lee-Thorp (1999) |
| C/C | 1455/ 1410 | A-type to B-type carbonates | $\nu_3(CO_3)$ A-type | 1200–1800 | Thompson et al. (2009) |
| $CO_3$/P | 872/ 1010 | $\nu_2(CO_3)$ B-type carbonate to phosphate | | | Thompson et al. (2013)<br>Ellingham et al. (2016) |
| Am/$C_1$ | 1640/ 1410 | Amide I to $\nu_3(CO_3)$ B-type carbonate | | | Kontopoulos et al. (2020) |
| FWHM | | Full width at half-maximun of the $\nu_3(PO_4)$ phosphate band | | 1150–890 | (Kimura-Suda and Ito 2017)<br>Hollund (2013) |
| AmIII/ P | 1270/ 1010 | Amide III to phosphate | Amide III C-N | 1290–1210 | (Chadefaux et al., 2009) (Leskovar et al., 2020) |
| Am/$C_2$ | 1640/ 872 | Amide I to $\nu_2(CO_3)$ B-type carbonate | $\nu_2(CO_3)$ B-type | 830–890 | Kontopoulos et al. (2020) |
| PHT | 625/ 610 | Phosphate high temperature. $OH^-$ groups to phosphate | $OH^-$ libration | | Thompson et al. (2013) |
| Cal/P | 712/ 1010 | Calcite to phosphate | $\nu_4(CO_3)$ | 730–700 | Dal Sasso et al. (2016) |

In our study, we present an analysis using nine different algorithms: neural networks (NNET), support vector machines (SVM), k-nearest neighbour (KNN), random forest (RF), decision trees using the C5.0 algorithm (DTC5.0), linear discriminant analysis (LDA), mixture discriminant analysis (MDA), partial least squares (PLS) and naïve Bayes algorithm (NB). These algorithms are a selection of those identified as the most powerful classificatory methods available (Lantz, 2013) which have been successfully employed in taphonomic analyses (Arriaza and Domínguez-Rodrigo, 2016; Domínguez-Rodrigo, 2019; Moclán et al., 2019). The use of different algorithms can be a useful tool to understand the variability of samples and results. If some of them show a perfect classification, only those algorithms that show worse results can be analysed by the researcher to improve the knowledge about the topic. An example of this is the correlation matrices, which will show the failures committed by the models and thus, which analysed samples are the most complicated (Moclán et al., 2020).

At the same time, the use of these algorithms provides a more reliable approximation to test statistical significance because all of them are mathematically different and they perform the classification of the samples in different ways. Thus, for example, we have included a neural network algorithm (NNET), two algorithms related to the use of decision trees (DTC5.0 and RF), or an algorithm based on the Bayes theorem in order to develop different approximations to the same problem. However, the functioning of the different ML algorithms differs mathematically, although all of them conduct the analyses in the same way. It is said that although there are clear differences among the algorithms that we used in this study, their application is the same, as can be seen below.

The samples were separated into two different parts: training (70% of the sample) and testing (30% of the sample). This methodology is used to check the reliability of a model, observing whether the tested model allows the correct classification of the sample. Furthermore, we have preprocessed the data when the algorithms were trained (centered and scaled data). We have used the mean values included in Table S1 to perform the analyses in the same way that when we developed the PCA.

Accuracy must be checked to interpret the data obtained by the model, which takes a value of 0–1 reflecting the quality of the classification test (i.e. 1 reflects a correct classification of the 100% of the sample).

Also, the kappa agreement index was calculated. It accounts for the possibility of a correct prediction occurring by chance alone, taking a value of −1 to 1, and with values of 0.8–1 reflecting results in very good agreement (Lantz, 2013). This index must be taken into account together with the accuracy. In the present analysis, the values of sensitivity (rate of true positives), specificity (rates of true negatives), and balanced accuracy (accuracy related to each analysed category) are also considered because they allow a complete evaluation of the results together with accuracy and kappa index. The combination of all these data is mainly useful if there is an imbalance in class classification (i.e. the number of samples per class should be similar to obtain more accurate models).

Cross-validation has been used with 10 folds and 10 repetitions to improve the quality of the analyses overcoming the problem of the overfitting of the models. In order to create accurate models, we have used the function "tuneLenght" of the 'caret' library (Kuhn et al., 2020) to create 10 different random models with different hyperparameter configurations of all the algorithms (except LDA because it does not allow the possibility of changing the configuration of the hyperparameters) which can be compared through kappa agreement index. Note that the final best tune model configuration (i.e. selected hyperparameters) has been included in the supplementary files for all of the algorithms.

Finally, we have included the use of a meta-algorithm (created with a NNET) that combines the classification of all the base learners previously developed. This technique is known as "ensemble learning" and it usually creates a better performance analysis due to the possibility of combining different algorithms which create classifications in clear different ways (Opitz and Maclin, 1999; Rokach, 2010; Sagi and Rokach, 2018). For this, it is important to know if there is not-correlation between the classification of the used algorithms. As can be seen in the supplementary files the correlation between the models is low or non-existence. We have used the function "modelCor" (Kuhn et al., 2020) of 'caret' library to identify the possible relation between the models. The NNET meta-learner has been created with a cross-validation controller and it has been repeated 10 times using the "tuneLenght" function.

In addition, different supplementary files (from Table S9 to Table S12) show the importance of the different variables in the analysis. In the case of NNET, RF, and DTC5.0, these tables show the

importance of all variables when they are tested, while the others show the importance considering the categories used (i.e. archaeological facies). It must be noted that each algorithm measures the importance in different ways but it is easy to understand the results because the larger the number is, the more important is the variable. Also, we have included all the confusion matrices generated by all the different algorithms to show how the results have been provided.

## 3. Results

### 3.1. ATR-FTIR and collagen extraction results

The results of the diagenetic parameters are shown in Fig. 3 and Table S1 for each bone sample. In the same way, Table S2 shows the results of surface bone analysis. The results are presented separating the organic and mineral phases.

*Organic phase:* The values obtained for the organic phase are shown through Am/P, AmIII/P and Nwt%, and Collagen wt%. Am/P ranges from 0 to 0.13 in facies *a*; from 0 to 0.01 in facies *tf*; from 0.03 to 0.16 and from 0.01 to 0.15 in facies *v* sector 100 and 200 respectively (Fig. 3). No value was recovered for facies *r(m)*, corresponding to calcined bones. AmIII/P ranges from 0 to 0.03 in facies *a*; from 0 to 0.02 in facies *v*200 and from 0 to 0.03 in facies *v*100. No values were obtained for the facies *r(m)* and *tf*. Taking into account the recovered amount in the extraction protocol, the average values for each facies show differences in preserved collagen amount. The bones samples from facies *a* preserve an average of 10.27 wt% of estimated collagen (10.99 wt% extracted), facies *v* retain 10.72 wt% of estimated collagen in *v*100 (10.02 wt% extracted) and 10.3 wt% of estimated collagen (8.78 wt% extracted) in *v*200. On the other hand, the facies *tf* preserves an average of 2.02 wt% of estimated collagen (2.06 wt% extracted). There is a clear difference between the unburned facies, which conserve around 10% of collagen

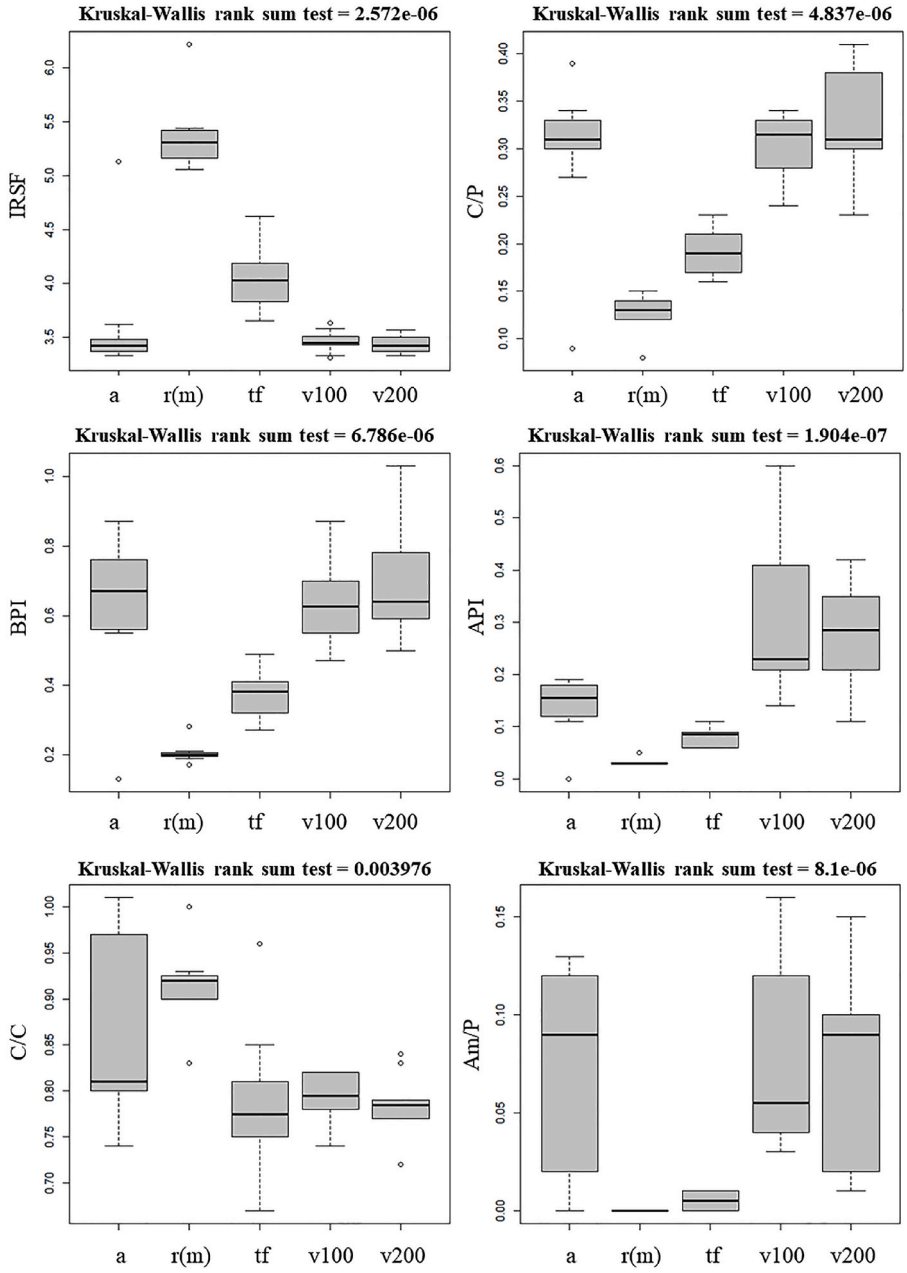


**Fig. 3.** Box plot of the diagenetic parameters from ATR-FTIR proposed in France et al. (2020) and Am/P. Infrared splitting factor (IRSF), carbonate to phosphate (C/P), type B carbonate to phosphate (BPI), type A carbonate to phosphate (API), A-type to B-type carbonate (C/C), Amide I to phosphate (Am/P).

and burned facies which are close to 2% or no collagen recovery. In addition, it is observed that in both facies *v* (not burned facies) the bone remains where cremations are absent present high percentages of collagen content. Further, the $Am/C_1$ and $Am/C_2$ indices show different results for each investigated facies. These parameters relate the amide I band to the B-type carbonate positions $\nu_3(CO_3^{2-})$ and $\nu_2(CO_3^{2-})$. In the unburned facies, values range from 0 to 0.77 for $Am/C_1$ and from 0 to 1.73 for $Am/C_2$. In the burned facies, values range from 0 to 0.21 for $Am/C_1$ and 0 to 0.32 for $Am/C_2$.

*Mineral phase:* Taking into account the preservation of bioapatite, the crystallinity index (IRSF) is also statistically different between burned and unburned facies (Fig. 3). IRSF ranges from 3.3 to 5.1 in remains from facies *a* (its tendency is 3.3–3.6 if we remove the only calcined remain); from 3.65 to 4.62 in facies *tf*; from 3.3 to 3.6 in facies *v* from sector 100 and from 3.3 to 3.5 for sector 200; and from 5.1 to 6.2 in facies *r(m)*. There is a clear difference in the distribution of the mean values which depends on whether the facies (and therefore the bones) were burned or not. Regarding FWHM ranges from 70.26 to 102.34 for facies *a*; from 65.2 to 76.12 for facies *tf;* from 76.93 to 96.36 and 77.84 to 100.12 for facies *v*100 and *v*200 respectively. Finally, we have obtained values from 57.9 to 74.08 for facies *r(m)*. Thereby, we observe a high degradation in the burned facies *tf* and *r(m)*.

The application of the Welch's ANOVA, Kruskal-Wallis and Wilcoxon (Cal/P) tests shows that statistically differences exist among the facies (Table S6; Table S7). However, these results can be explained better if the pairwise comparison among groups is done. It was observed that the bone remains of the unburned facies (facies *v*100 and facies *v*200) and reelaborated facies (facies *a*) do not have statistically significant differences for the Am/P, IRSF, C/P, BPI, C/C, Cal/P, $CO_3$/P, $Am/C_1$, PHT, FWHM, $Am/C_2$ indices (Table S7). However, the API index establishes significant differences between the bone remains of facies *a* and *v* (p-value = 0.0085 for *v*100; p-value = 0.0213 for *v*200). Nevertheless, it does not reflect significant differences between the two facies *v*. These results indicate a difference in bone preservation in both facies in relation to A-type carbonates. However, there was no significant difference between facies *a* and facies *r(m)* (p-value = 0.0592) for the API index.

Regarding the bone remains of the burned facies (facies *r(m)* and facies *tf*), we found significant differences for the indices that attend to crystallinity and carbonates in the bioapatite, as well as the incorporation of calcite ($CaCO_3$): IRSF (p-value = 0.001), C/P (p-value = 0.0074); BPI (p-value = 0.0104); API (p-value = 0.0054); Cal/P (p-value = 0.0043). The PHT index, relative to the libration of $OH^-$ groups due to high temperatures (Thompson et al., 2013; Ellingham et al., 2016), has also made possible to differentiate the facies *r(m)* and *tf* (p-value = 0.0033). Similarly, all the bones recovered from the facies *r(m)* show a stage 5 burnt, while the facies *tf* shows stages 3 and 4 (Table S2). Due to the coloration and the PHT index, the remains of the facies *tf* yield an estimated temperature around 300 °C. The remains of the facies *r(m)* yield estimated temperatures close to 700 °C since hydroxyl groups have been observed with the 3570 $cm^{-1}$ band in the calcined bone remains from facies *r(m)*. The 712 $cm^{-1}$ band corresponding to $\nu_4(CO_3^{2-})$ is found in all the calcined bone remains of the facies *r(m)* and one bone sample from facies *a* (Table S1*)*. This band is related to the presence of secondary calcite due to the incorporation of exogenous carbonates in the burial environment. Table S1 shows the percentages of secondary calcite in each sample obtained from the Cal/P index following the methodology of Dal Sasso et al. (2016). These values correspond from 9.2 wt% to 16.9 wt% of secondary calcite precipitate in bone remains from facies *r(m)*.

Finally, carbonate and phosphate ratio shows a correlation with the crystallinity index ($r^2 = 0.78$) (Fig. 4). This relationship is indicative of the recrystallization degree of the bones in the different facies. The greatest alteration of the bone remains can be observed in the burned facies. In the unburned and reelaborated facies, we cannot detect a difference in recrystallization despite the temporal range difference (note the temporal difference in both facies *v*).

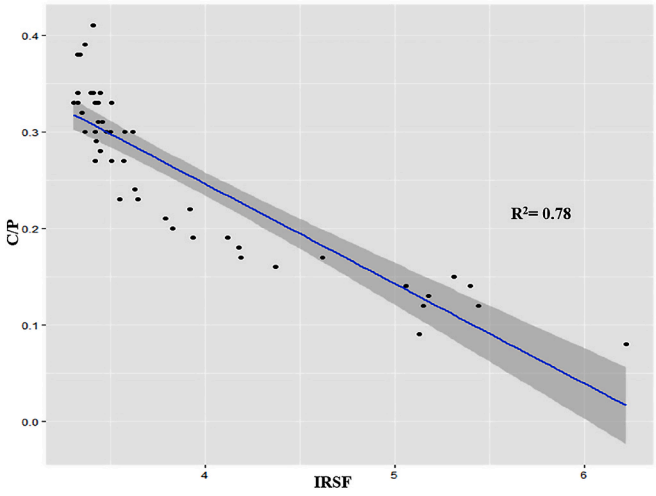


**Fig. 4.** Carbonate to phosphate (C/P) ratio and crystallinity index (IRSF) showing linear regression.

### 3.2. PCA results of the ATR-FTIR spectra

The PCA explained 80.94% of the variance through two principal components (Fig. 5; Table S8). The facies distribution showed 3 well-defined groups between facies *tf*, facies *r(m),* and the unburned facies. The facies are distributed throughout the PCA, showing a reelaborated facies that does not create a clear group. The variables that strongly contribute to this distribution are Am/P, IRSF, AmIII/P, C/P, BPI, and $Am/C_1$.

According to the values of PC1-loading and PC2-loading (Fig. 5), IRSF and PHT are significant variables to discriminate facies *r(m)* and *tf*. In addition, these two facies are separated from each other due to the values of the carbonates. In the case of facies *v*100 and *v*200, they are located on the left side of the abscissas axis because of the indices related to the organic phase and carbonates indices, although the PCA does not seem to show differences between them.

### 3.3. Facies classification based on Machine Learning

The ML analysis shows clear differences depending on the applied algorithms (Table 3). Most of the algorithms provide inconclusive results with low classification values. First, SVM shows the worst classification rate (accuracy = 0.429; kappa = 0.282) which has correctly classified less than half of the testing set. NNET, kNN, NB, LDA, PLS, and DTC5.0 show better results than SVM but they are still inconclusive (accuracy = < 0.643). However, RF and MDA show a quite strong classification presenting an accuracy value of 0.786 (kappa = 0.731).

When the confusion matrices (Table S9) are analysed, a clear relation between the results of the different algorithms can be seen. In general terms (except for SVM, NB, and DTC5.0), all the algorithms correctly classify all the samples related to the burned facies; *r(m)* is correctly classified by all the algorithms while 1 sample is incorrectly classified by SVM, NB, and DTC5.0) and they make errors when bone samples from the unburned and reelaborated facies are classified (note that only DTC5.0 has perfectly classified the facies *a*).

When all algorithms are ensembled the results are significatively increased and they show a perfect classification rate (accuracy = 1; kappa = 1). This means that the ensemble model has correctly classified all the samples included in the testing dataset. The ensemble model has improved the previous results due to the low correlation rates provided by the different algorithms (Table 4).

In general, all the correlations are lower than 0.5 and correlation is only present (~0.53) between MDA and LDA, NB and PLS, LDA and PLS, and DTC5.0 and RF. This aspect has probably increased the accuracy of

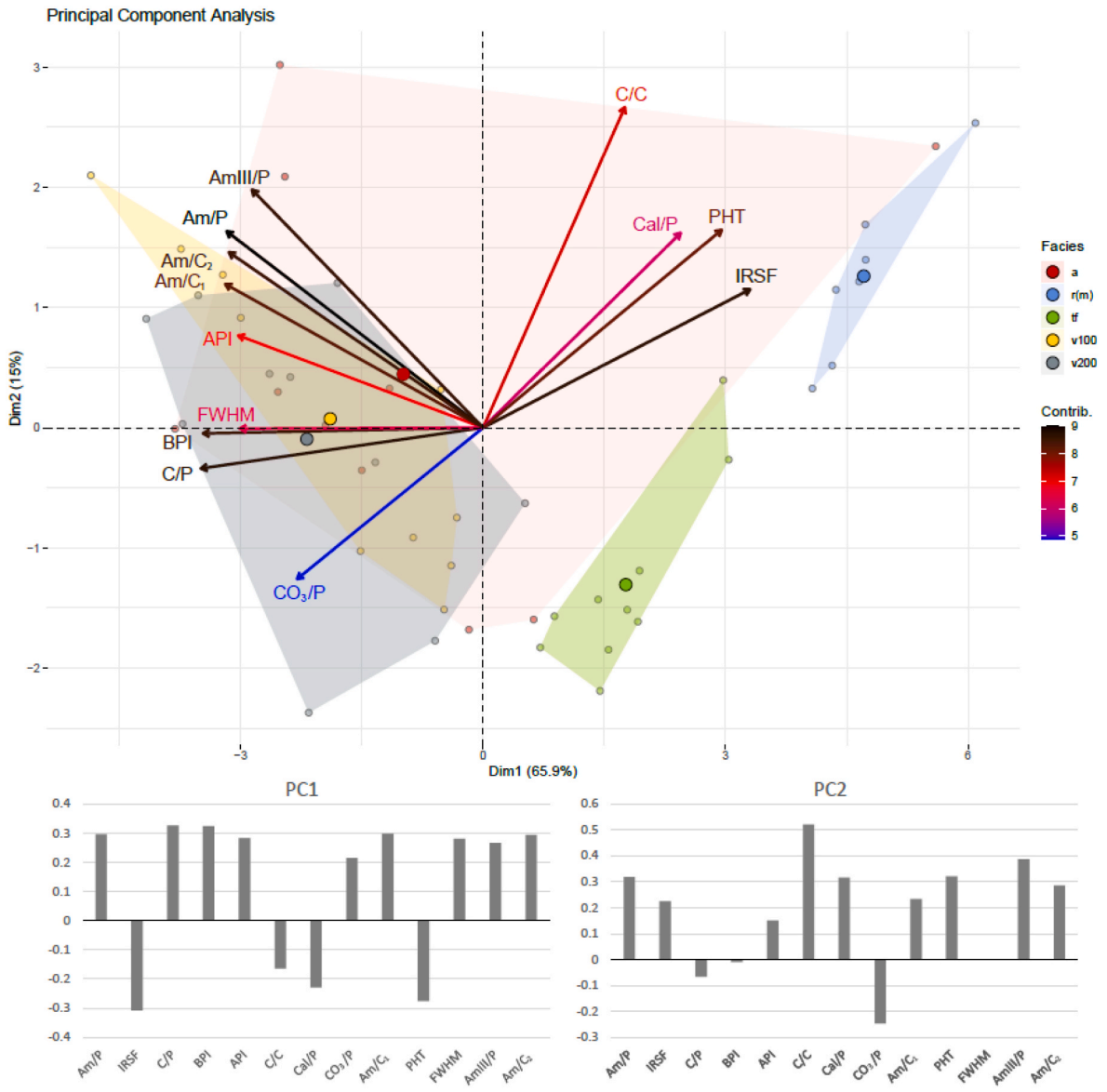


**Fig. 5.** Principal component analysis (PCA) showing the dispersion of the samples by the diagenetic parameters. The darker a vector is, the more it contributes to the spatial distribution of the components. Note that the length of the vector is showing the real contribution of them to the PCA performance. At the bottom, the loadings of the PC1 and PC2 can be seen.

**Table 3**
Accuracy and kappa values provided by the ML algorithms used to classify the different facies. Note that the values provided by the stacking model are also included in the tables.

| | Accuracy | Kappa | Accuracy Lower | Accuracy Upper |
|---|---|---|---|---|
| **NNET** | 0.571 | 0.462 | 0.289 | 0.823 |
| **SVM** | 0.429 | 0.282 | 0.177 | 0.711 |
| **kNN** | 0.571 | 0.462 | 0.289 | 0.823 |
| **RF** | 0.786 | 0.731 | 0.492 | 0.953 |
| **MDA** | 0.786 | 0.731 | 0.492 | 0.953 |
| **NB** | 0.5 | 0.372 | 0.23 | 0.77 |
| **LDA** | 0.571 | 0.462 | 0.289 | 0.823 |
| **PLS** | 0.571 | 0.462 | 0.289 | 0.823 |
| **DTC5.0** | 0.643 | 0.551 | 0.351 | 0.872 |
| **Ensemble (NNET)** | 1 | 1 | 0.768 | 1 |

**Table 4**
Correlation matrices showing the correlation between the different ML algorithms used in this study. Correlated values are shown in red and bold. Note that most of the algorithms are uncorrelated and that the correlated cases show weak relations.

| Correlation matrices | | | | | | | | |
|---|---|---|---|---|---|---|---|---|
| | NNET | SVM | kNN | RF | MDA | NB | LDA | PLS |
| **SVM** | 0.18 | – | – | – | – | – | – | – |
| **kNN** | 0.21 | 0.29 | – | – | – | – | – | – |
| **RF** | 0.29 | 0.22 | 0.23 | – | – | – | – | – |
| **MDA** | 0.38 | 0.37 | 0.36 | 0.10 | – | – | – | – |
| **NB** | 0.12 | 0.03 | 0.43 | 0.37 | 0.16 | – | – | – |
| **LDA** | 0.39 | 0.42 | 0.37 | 0.19 | **0.55** | 0.25 | – | – |
| **PLS** | 0.49 | 0.20 | 0.38 | 0.35 | 0.45 | **0.52** | **0.53** | – |
| **DTC5.0** | 0.33 | −0.01 | 0.22 | **0.53** | 0.17 | 0.44 | 0.33 | 0.48 |

the ensemble model because even algorithms that are mathematically similar (e.g. DTC5.0 and RF) provide lower correlation values.

It must be noted that the 9 most important variables used to train the ensemble model are related with the facies *v*100 and *v*200, which are incorrectly classified by the base learners (Figure S3). In other words, the most important variables used to train the ensemble model are

related to the worst classified samples by the base learners.

Regarding the importance of the used variables, it must be noted that there is a clear variability between the models. However, it can be noted that API, BPI, C/P are the more important variables from a general point of view. At the same time, other variables as $CO_3$/P, C/C, AmIII/P, and Cal/P are the worst variables in most of the models. In any case, it seems that API can be the most important variable when NNET, RF, and DTC5.0 are used (Table S10). We note that the variables related to carbonates to phosphates indices have been able to classify facies *v* and *a* through RF, MDA, and NNET (Table S10 and Table S11).

## 4. Discussion

Establishing the differences between *fumier* facies from bone remains is important to understand its provenance as a result of the taphonomic reelaboration related to the own *fumier* (heap and burnt sediments to clean and to deworm livestock areas). Our results have shown that it is possible to classify *fumier* facies with different taphonomic stories through diagenetic parameters using ATR-FTIR spectroscopy. We used five facies showing the variety of *fumier* conditions: two unburned facies, one reelaborated facies, and two burned facies at different temperatures. The *fumier* sequence from El Mirador cave is an exceptionally well-preserved example of Holocene *fumier* and it is a suitable site to test our methodology, which is applicable to the *fumier* deposits present in other shepherds' caves of the Mediterranean area (Brochier, 1992; Angelucci et al., 2009; Oms et al., 2013; Polo et al., 2016; Vergès et al., 2016; Burguet-Coca et al., 2020). As Angelucci et al. (2009) noted, *fumier* deposits might keep common sedimentological features, and this will allow recognizing similar diagenetic trajectories on different *fumier* sites.

In the context of facies *a* (yellowish-brown clayey silt layer), the bone samples have shown good preservation of collagen amount and bioapatite crystals. That is, in the range of well-preserved archaeological bones (Kendall et al., 2018; France et al., 2020). The crystallinity is related to the carbonate amount, providing evidence of an existing close relationship with the reached temperature affecting the bones samples. Facies *a* provides good preservation values, although a slight high carbonate amount has been detected comparing data provided by France et al. (2020). That is to say, there has been an incorporation of carbonate ions ($CO_3^{2-}$) in the crystal lattice which affects the mineral structure and crystal size (Shemesh, 1990; Lee-Thorp and van der Merwe, 1991; Trueman et al., 2008). However, this absorption does not result in the incorporation of $CaCO_3$. In addition, the API and C/C indices, which take into account the A-type carbonates, have shown that the conditions of this facies are different from those of the unburned facies (Fig. 3). This is important because it has been suggested that A-type carbonate substitution could appear when water is excluded from the burial environment (Bayarı et al., 2020). This means that a reelaborated context leads to taphonomic processes of its own and, therefore, the reelaborated facies could be differentiated. In summary, facies *a* is characterized by a high percentage of collagen, high C/P ratio and low IRSF in no cremated bones remains.

Facies *v* (layers of clayey loam) presents the highest collagen contents and the best-preserved crystallinity for both sectors 100 and 200. This fits well with the expected relationship between high organic content and its influence on crystallinity (Hedges, 2002). They can therefore be proposed as good facies for proteomics and both collagen and bioapatite isotope analysis. However, we have detected a slight increase of C/P in some cases, which is responsible for high crystal disorder (Dal Sasso et al., 2018), so samples from these facies should be pre-screening individually before proceeding to isotopic analysis. In this type of facies we identify boiled bones. However, this taphonomic modification in the *fumier* deposits needs to be further investigated. Boiled bones are identifiable at the macroscopic level following the criteria proposed by several authors (Nicholson, 1996, 1998; Botella, 2000; Martin-Rodriguez, 2015). In our results, boiled remains have presented a good amount of preserved collagen confirming what has already been noted in other studies (Roberts et al., 2002; Koon et al., 2003, 2010: Munro et al., 2007), even recording Amide III (Chadefaux et al., 2009; Bobbroff et al., 2016; Leskovar et al., 2020). Likewise, we would like to highlight that the C/P ratio is slightly high in these remains. This could be related to the highly organic facies *v* itself or the taphonomic modification of boiling. In summary, facies *v* bones are characterised by low IRSF crystallinity, high carbonate content, and high collagen content. These values are close to modern bone so facies *v* can be considered a well-preserved context in terms of mineral conservation and organic amount.

About facies *tf*, the conservation of collagen amount in bones is very homogeneous, close to 3 wt%, which indicates a recrystallization increasing the IRSF. That is, the bones have received a thermal impact close to carbonization at 300 °C (Lebon et al., 2010; Cáceres, 2002). These results could be related to postdepositional cremation and the cleaning and formation dynamics of the *fumier* (Angelucci et al., 2009). The reduced carbonate content is in line with this thermal alteration as it has been observed in other experimental works (Lebon et al., 2010; Marques et al., 2018). The bones of the facies *tf* are characterised by a high crystallinity index and reduced carbonate and organic content values.

The facies *r(m)* is characterized by light brown massive accumulations of ash. The crystallinity index obtained in the bone remains is close to 5 with complete degradation of collagen. The exposure of a bone to high temperatures can be defined by ATR-FTIR, showing that in these facies the bones reached temperatures close to 700 °C (Berzina-Cimdina and Borodajenko, 2012; Marques et al., 2018). The carbonate content is very low due to the significant loss of the carbonate fraction of bioapatite during cremation (Stiner et al., 1995; Thompson et al., 2013; Marques et al., 2018), hence the bones are not really suitable for C and O stable isotope analyses. Secondary calcite has only been observed in this facies and in a bone remain from facies *a* (reelaborated facies). These results are attributed to the ashy sediment composition, showing the need to include sediment analysis in this type of work (Polo-Diaz et al., 2010).

The application of PCA to the ATR-FTIR spectra allowed the differentiation of the facies. On the one hand, the burned facies *tf* and *r(m)* are differentiated by temperature reached. On the other hand, it could be understood that facies *v* from different sectors share the same values and the same component space. Facies *a* fills almost all the component space and does not form a group of its own, results which support the interpretation of a reelaborated facies. Overall, our PCA analysis indicates that the most important variables for facies differentiation are the IRSF crystallinity index and the indices that analyse the organic phase and carbonates: Am/P, IRSF, AmIII/P, C/P, BPI, and Am/$C_1$. It must be noted that the PCA seems to show that IRSF and PHT are important variables to discriminate facies *r(m)* and *tf*. In addition, these two facies (located in the right part of the abscissas axis) seem to be separated between them due to the different values of $CO_3$/P and others like C/P and BPI.

In the case of the facies *v*100 and *v*200 they are in the same area of the left part of the abscissas axis and they seem to be not differentiable between them. The PCA shows that the indices relative to organic phase and carbonates are the ones that are placing these facies in the left part of the plot.

We have obtained results with lower values for the C/P and Am/$C_1$ indices in burned bones than those reported in other experimental data (Thompson et al., 2013; Ellingham et al., 2016). This suggests a continued degradation of proteins and carbonates during bone diagenesis.

It is therefore relevant to pay attention to the impact of fire when studying bone diagenesis in *fumier* contexts. The last burnt episode and formation of a facies trigger an initial phase for early bone diagenesis at the time of burial. It is necessary to take into account the reelaboration produced by shepherds (accumulation and mixing of sediments before burning) and not to frame the entire process in the fossil-diagenetic

phase. This approach helps to understand the issue of synchronicity in the assemblage and to discriminate between anthropogenic or natural reelaboration, helping to make better inferences about archaeological assemblages.

Our results also help to set suitable standard procedures through ATR-FTIR and bone diagenesis studies. This is something desirable for authors that we follow in terms of method procedure (Lebon et al., 2016; Kontopoulos et al., 2018) and the use of analytical indices (France et al., 2020). Likewise, we agree that C/P is an index that presents a large source of variation between sample groups (France et al., 2020; Bayarı et al., 2020). Furthermore, our results show that BPI, C/C, and API are important variables in facies differentiation with the NNET, RF, and DTC5.0 algorithms. API, in particular, should be strongly considered in *fumier* contexts, as it is a good indicator between facies where A-type carbonates may dominate, which controls the properties of apatitic minerals under non-physiological conditions (Madupalli et al., 2017).

Nevertheless, it must be noted that the use of the different ratios does not allow us to differentiate the *fumier* facies unless powerful statistical approximations are used. When all parameters are analysed separately, or at the same time, with box plots and PCA, only the two burned facies are identified. However, when ML algorithms are used, and more specifically when Ensemble Learning is used, the classification of the different facies is perfect and allows us to differentiate within facies here investigated.

However, we must point out that there are limitations in this study due to the sample size. In general, when ML techniques are applied, large samples are used. In this case, the destructive nature of the collagen extraction method prevented a sample increment (Longin, 1971; Bocherens et al., 1991). However, it can be seen (Table S1) that minimally-destructive methods such as infrared spectroscopy allow accurate measurement of the collagen content (Trueman et al., 2004; Lebon et al., 2016; Sponheimer et al., 2019; Kontopoulos et al., 2020), being a useful tool in assemblages that are often fragmented such as *fumiers*. Thus, the ML results should be interpreted as preliminary. However, all our results (not only ML results) are statistically consistent, therefore we believe that if we increase the sample, the results will be the same but with one exception: the base learners (e.g. RF, MDA) will likely produce more accurate models and the ensemble model will be exactly the same. For this reason, we think that these results are relevant for future works at least for the following aspects.

Firstly, they bring the possibility of differentiating between facies that have the same type of taphonomic origin like the unburned facies *v* from 100 to 200 sectors. The PCA showed that it is easier to separate the burned facies to classify them. However, facies with similar sedimentological features (facies *v*) or with reelaborated remains (facies *a*) present some problems if unsupervised statistical methods are used. Only through the use of ensemble learning it has been possible to distinguish all facies among them, showing that the values relative to carbonates to phosphates are the most important at classifying (Table S8 and Table S9); secondly, they show how the ML approach can provide some possibilities in the future for the identification of taphonomic trajectories in independent archaeological sites and contexts; and last, these type of methods can provide a solution to identify the origin of some non-contextualized artefacts from archaeological sites.

While it is true that further investigation around the diagenetic study of *fumiers* is required, some studies have indicated good preservation of bone surfaces in compost heaps and dung layers (Nicholson, 1996, 1998; Martín-Rodríguez, 2015). Thus, we note that the processes involved in layers composed of dung and organic matter are complex but do not result in an aggressive burial environment.

Considering our results, bone diagenesis analysis can improve our capacity to analyse complex sequences as *fumier* (Macphail et al., 1997; Golberg and Macphail 2006; Angelucci et al., 2009; Friesem 2016). Facies sequences are the result of the accumulation process produced by the volume reduction by fire, which can affect 90% of the initial volume (Acovitsioti-hameau et al., 1999; Shahack-Gross et al., 2005; Vergès et al., 2016), concentrating, mixing, and fragmenting among others the bone remains (Vergès 2011; Martín-Rodríguez and Vergès 2016). This reduction process can be combined with other taphonomic processes generating complex stratigraphic sequences and depositional patterns. Our results allow us to identify bones differences related by diagenetic parameters carried out in each facies, to clarify interpretations about the origin of each facies, palimpsest, and the bones they include. The facies distinction through ATR-FTIR and bones is not exclusive to the *fumier* identified in El Mirador cave. Although this preliminary work has indeed been carried out with a small number of samples, it is important to create classification methods incorporating information from other *fumier* deposits (Table S11). Angelucci et al. (2009) already pointed out that the sedimentological conditions of the *fumiers* are quite similar among them. This supports the idea that there must be similar diagenetic trajectories that can be compared. Therefore, it is necessary to obtain a large database to be able to generate models between *fumiers*. This can be a useful tool for analysing bone assemblages, recognizing the common origin of the assemblages and assessing the stage of conservation they present.

## 5. Conclusion

This study constitutes the first attempt to address bone diagenesis in *fumier* contexts using ATR-FTIR. We have shown the different preservation of five *fumier's* facies through the molecular information of the bones from El Mirador cave, which is an exceptional example of this type of context. The following are the main conclusions reached by the study:

A) *Fumier*'s facies have its own diagenetic features and can be differentiated through the molecular information of the bones. While no differences in preservation were noted attending its chronology of bone assemblage, significant differences have been attested considering its origin by facies features. The parameters used with ATR-FTIR make it possible to assess the incidence of fire in each facies beyond the colouring of the bone remains.

B) In a *fumier* context, the facies *v*, with good preservation of organic and bioapatite material, are a telling example for isotopic and paleoproteomic studies. Therefore, it is important to delve into bone diagenesis studies in this type of context and to do not dismiss the bone remains directly because of the incidence of fire. Even then, bone samples must be evaluated individually due to the increase in $CO_3^{2-}$ ions detected.

C) Diagenetic parameters and algorithms through ML provide a new decisive method to identify and classify *fumier*'s facies. It is even possible to understand that a reelaborated assemblage has diagenetic characteristics of its own. Parameters through ATR-FTIR and ML have allowed defining that the carbonate variables API, BPI, and C/P are the most important variables to discriminate differences between facies. While through PCA the most significant variables were Am/P, IRSF, AmIII/P, C/P, BPI, and Am/$C_1$.

D) ATR-FTIR is an economical, minimally-destructive and efficient tool to characterize archaeological bones and teeth assemblages and pre-screening samples for further isotopic or proteomic analysis.

E) El Mirador cave provides an outstanding reference among *fumier* sites for bone diagenesis studies. It offers an exceptional opportunity to explore new methods in bone Taphonomy which can be applied to other *fumier* assemblages in Holocene contexts from the Mediterranean basin. Monitoring the processes affecting the bone assemblages will improve the knowledge of the activities carried out by the herders in the caves and rock shelters.

## Declaration of competing interest

The authors declare that they have no known competing financial

interests or personal relationships that could have appeared to influence the work reported in this paper.

## Acknowledgements

This research is framed in the PGC 2018-093925-B-C32 (MICINN-Feder), the 2017SGR1040 (AGAUR), and the 2019PFR-URV-91 (URV) projects. Research at IPHES is framed in the CERCA program. This research was supported by the Ministry of Science and Innovation, Spanish Government through the "María de Maeztu" excellence accreditation (CEX 2019-000945-M). We would like to thank the Atapuerca team and, specially, the El Mirador cave team for their collaboration. Also, we would like to thank Dr. Matthieu Lebon and Dr. Xavier Gallets for the laboratory training during the master's mobility of HDV. Finally, we would like to thank the team area of microscopy and nanometric techniques of the SRCiT of the URV for their advice. The research of CT was supported by the Ministry of Science and Innovation, Spanish Government through the "Ramon y Cajal" programme (RYC2020-029404-I). AB-Cs research is funded by Universitat Rovira i Virgili (URV) and "NextGenerationEU" funds of the European Union through the plan for Recovery, Transformation and Resilience of the Ministry of Universities, Spanish Government (2021 URV-MS-04). AM is funded by a grant from the Junta de Castilla y León financed in turn by the European Social Funds through the Consejería de Educación (BDNS 376062). We would like to thank two anonymous reviewers and editor for their suggestions that greatly improved this manuscript.

## Appendix A. Supplementary data

Supplementary data to this article can be found online at https://doi.org/10.1016/j.jas.2022.105582.

## References

Acovitsioti-hameau, A., Brochier, J.E., Hameau, P., 1999. Temoignages et marqueurs du pastoralisme actuel en grece: une ethnographie des gestes et des restes et les applications archeologiques correlees. Ethnologhia 6 (7), 93–135.

Angelucci, D.E., Boschian, G., Fontanals, M., Pedrotti, A., Vergès, J.M., 2009. Shepherds and karst: the use of caves and rock-shelters in the Mediterranean region during the Neolithic. World Archaeol. 41, 191–214. https://doi.org/10.1080/00438240902843659.

Argant, J., Heinz, C., Brochier, J.-L., 1991. Pollens, charbons de bois et sédiments : l'action humaine et la végétation, le cas de la grotte d'Antonnaire (Montmaur-en-Diois, Drôme). Rev. d'Archéométrie 15, 29–40. https://doi.org/10.3406/arsci.1991.1255.

Arriaza, M.C., Domínguez-Rodrigo, M., 2016. When felids and hominins ruled at Olduvai Gorge: a machine learning analysis of the skeletal profiles of the non-anthropogenic Bed I sites. Quat. Sci. Rev. 139, 43–52. https://doi.org/10.1016/J.QUASCIREV.2016.03.005.

Bayarı, S.H., Özdemir, K., Sen, E.H., Araujo-Andrade, C., Erdal, Y.S., 2020. Application of ATR-FTIR spectroscopy and chemometrics for the discrimination of human bone remains from different archaeological sites in Turkey. Spectrochim. Acta Part A Mol. Biomol. Spectrosc. 237 https://doi.org/10.1016/j.saa.2020.118311.

Beasley, M.M., Bartelink, E.J., Taylor, L., Miller, R.M., 2014. Comparison of transmission FTIR, ATR, and DRIFT spectra: implications for assessment of bone bioapatite diagenesis. J. Archaeol. Sci. 46, 16–22. https://doi.org/10.1016/j.jas.2014.03.008.

Berzina-Cimdina, L., Borodajenko, N., 2012. Research of calcium phosphates using FTIR spectroscopy. Infrared Spectrosc. - Mater. Sci. Eng. Technol. 12, 251–263.

Bobroff, V., Chen, H.H., Javerzat, S., Petibois, C., 2016. What can infrared spectroscopy do for characterizing organic remnant in fossils? TrAC Trends Anal. Chem. (Reference Ed.) 82, 443–456. https://doi.org/10.1016/j.trac.2016.07.005.

Bocherens, H., Fizet, M., Mariotti, A., Lange-Badre, B., Vandermeersch, B., Borel, J.P., Bellon, G., 1991. Isotopic biogeochemistry (13C,15N) of fossil vertebrate collagen: application to the study of a past food web including Neandertal man. J. Hum. Evol. 20, 481–492. https://doi.org/10.1016/0047-2484(91)90021-M.

Bosch, P., Alemán, I., Moreno-Castilla, C., Botella, M., 2011. Boiled versus unboiled: a study on Neolithic and contemporary human bones. J. Archaeol. Sci. 38, 2561–2570. https://doi.org/10.1016/j.jas.2011.04.019.

Botella, M.C., Alemán, I., Brobeil, S., 2000. Los Huesos Humanos: Manipulación Y Alteraciones. Ediciones Bellaterra, Barcelona.

Brochier, J.E., 2002. Les sédiments anthropiques. Méthods d'etude et perpectives. Paris. In: Miskovswi, J. (Ed.), Géologie de La Préhistoire: Méthodes, Techniques, Applications, 453–377.

Brochier, J.E., Villa, P., Giacomarra, M., Tagliacozzo, A., 1992. Shepherds and sediments: geo-ethnoarchaeology of pastoral sites. J. Anthropol. Archaeol. 11, 47–102. https://doi.org/10.1016/0278-4165(92)90010-9.

Brochier, J.E., 1991. Géoarchéologie du monde agropastoral. In: Colin, Armand (Ed.), Pour une Archéologie Agraire. À la croisée des sciences de l'homme et de la nature, pp. 303–322. Paris.

Burguet-Coca, A., Polo-Díaz, A., Martínez-Moreno, J., Benito-Calvo, A., Allué, E., Mora, R., Cabanes, D., 2020. Pen management and livestock activities based on phytoliths, dung spherulites, and minerals from Cova Gran de Santa Linya (Southeastern pre-Pyrenees). Archaeol. Anthropol. Sci. 12 https://doi.org/10.1007/s12520-020-01101-6.

Cabanes, D., Burjachs, F., Expósito, I., Rodríguez, A., Allué, E., Euba, I., Vergès, J.M., 2009. Formation processes through archaeobotanical remains: the case of the Bronze Age levels in El Mirador cave, Sierra de Atapuerca, Spain. Quat. Int. 193, 160–173. https://doi.org/10.1016/j.quaint.2007.08.002.

Cáceres, I., Lozano, M., Saladié, P., 2007. Evidence for Bronze age cannibalism in el mirador cave (Sierra de Atapuerca, burgos, Spain). Am. J. Phys. Anthropol. 133, 899–917. https://doi.org/10.1002/ajpa.

Cáceres, I., 2002. Tafonomía de yacimientos antrópicos en karst. Complejo Galería (Sierra de Atapuerca, burgos), Vanguard cave (Gibraltar) y Abric Romaní (Capellades, Barcelona). Universitat Rovira i Virgili.

Chadefaux, C., Hô, A. Le, Bellot-gurlet, L., Ina, R., 2009. Curve-Fitting micro-atr-ftir studies of the amide I and ii bands of type I collagen in. e-Preservation Sci. 129–137.

Chowdhury, M.P., Choudhury, K.D., Bouchard, G.P., Riel-Salvatore, J., Negrino, F., Benazzi, S., Slimak, L., Frasier, B., Szabo, V., Harrison, R., Hambrecht, G., Kitchener, A.C., Wogelius, R.A., Buckley, M., 2021. Machine learning ATR-FTIR spectroscopy data for the screening of collagen for ZooMS analysis and mtDNA in archaeological bone. J. Archaeol. Sci. 126, 105311. https://doi.org/10.1016/j.jas.2020.105311.

Collins, M.J., Nielsen-Marsh, C.M., Hiller, J., Smith, C.I., Roberts, J.P., Prigodich, R.V., Wess, T.J., Csapo, J., Millard, A.R., Turner-Walker, G., 2002. The survival of organic matter in bone: a review. Archaeometry 44, 383–394. https://doi.org/10.1111/1475-4754.t01-1-00071.

Courtenay, L.A., Yravedra, J., Huguet, R., Aramendi, J., Maté-González, M.Á., González-Aguilera, D., Arriaza, M.C., 2019. Combining machine learning algorithms and geometric morphometrics: a study of carnivore tooth marks. Palaeogeogr. Palaeoclimatol. Palaeoecol. 522, 28–39. https://doi.org/10.1016/j.palaeo.2019.03.007.

Dal Sasso, G., Asscher, Y., Angelini, I., Nodari, L., Artioli, G., 2018. A universal curve of apatite crystallinity for the assessment of bone integrity and preservation. Sci. Rep. 8, 12025. https://doi.org/10.1038/s41598-018-30642-z.

Dal Sasso, G., Lebon, M., Angelini, I., Maritan, L., Usai, D., Artioli, G., 2016. Bone diagenesis variability among multiple burial phases at Al Khiday (Sudan) investigated by ATR-FTIR spectroscopy. Palaeogeogr. Palaeoclimatol. Palaeoecol. 463, 168–179. https://doi.org/10.1016/j.palaeo.2016.10.005.

Dal Sasso, G., Maritan, L., Usai, D., Angelini, I., Artioli, G., 2014. Bone diagenesis at the micro-scale: bone alteration patterns during multiple burial phases at Al Khiday (Khartoum, Sudan) between the Early Holocene and the II century AD. Palaeogeogr. Palaeoclimatol. Palaeoecol. 416, 30–42. https://doi.org/10.1016/j.palaeo.2014.06.034.

Dominguez-Rodrigo, M., Fernández-López, S., Alcalá, L., 2011. How can taphonomy be defined in the XXI century? J. Taphon. 9, 1–13.

Domínguez-Rodrigo, M., 2019. Successful classification of experimental bone surface modifications (BSM) through machine learning algorithms: a solution to the controversial use of BSM in paleoanthropology? Archaeol. Anthropol. Sci. 11, 2711–2725. https://doi.org/10.1007/s12520-018-0684-9.

Domínguez-Rodrigo, M., Baquedano, E., 2018. Distinguishing butchery cut marks from crocodile bite marks through machine learning methods. Sci. Rep. 8, 1–8. https://doi.org/10.1038/s41598-018-24071-1.

Egeland, C.P., Domínguez-Rodrigo, M., Pickering, T.R., Menter, C.G., Heaton, J.L., 2018. Hominin skeletal part abundances and claims of deliberate disposal of corpses in the Middle Pleistocene. Proc. Natl. Acad. Sci. U. S. A. 115, 4601–4606. https://doi.org/10.1073/pnas.1718678115.

Ellingham, S.T.D., Thompson, T.J.U., Islam, M., 2016. The effect of soft tissue on temperature estimation from burnt bone using fourier transform infrared spectroscopy. J. Forensic Sci. 61, 153–159. https://doi.org/10.1111/1556-4029.12855.

Euba, I., Allué, E., Burjachs, F., 2016. Wood uses at el mirador cave (Atapuerca, burgos) based on anthracology and dendrology. Quat. Int. 414, 285–293. https://doi.org/10.1016/j.quaint.2015.08.084.

Expósito, I., Burjachs, F., 2016. Taphonomic approach to the palynological record of burnt and unburnt samples from El Mirador Cave (Sierra de Atapuerca, Burgos, Spain). Quat. Int. 414, 258–271. https://doi.org/10.1016/j.quaint.2016.01.051.

Fernández-López, S., 1991. Taphonomic concepts for a theoretical biochronology. Rev. Esp. Palaontol. 6, 37–49.

Fernández-López, S.R., 2006. Taphonomic alteration and evolutionary taphonomy. J. Taphon. 4, 111–142.

France, C.A.M., Sugiyama, N., Aguayo, E., 2020. Establishing a preservation index for bone, dentin, and enamel bioapatite mineral using ATR-FTIR. J. Archaeol. Sci. Reports 33, 102551. https://doi.org/10.1016/j.jasrep.2020.102551.

Friesem, D.E., 2016. Geo-ethnoarchaeology in action. J. Archaeol. Sci. 70, 145–157. https://doi.org/10.1016/j.jas.2016.05.004.

Goldberg, P., Macphail, R.I., 2006. Practical and Theoretical Geoarchaeology. Blackwell publishing, Victoria.

Gur-Arieh, S., Shahack-Gross, R., Maeir, A.M., Lehmann, G., Hitchcock, L.A., Boaretto, E., 2014. The taphonomy and preservation of wood and dung ashes found in archaeological cooking installations: case studies from Iron Age Israel. J. Archaeol. Sci. 46, 50–67. https://doi.org/10.1016/j.jas.2014.03.011.

Grunenwald, A., Keyser, C., Sautereau, A.M., Crubézy, E., Ludes, B., Drouet, C., 2014. Novel contribution on the diagenetic physicochemical features of bone and teeth minerals, as substrates for ancient DNA typing. Anal. Bioanal. Chem. 406, 4691–4704. https://doi.org/10.1007/s00216-014-7863-z.
Hedges, R.E.M., 2002. Bone diagenesis: an overview of processes. Archaeometry 44, 319–328.
Hollund, H.I., Ariese, F., Fernandes, R., Jans, M.M.E., Kars, H., 2013. Testing an alternative high-throughput tool for investigating bone diagenesis: ftir in attenuated total reflection (atr) mode. Archaeometry 55, 507–532. https://doi.org/10.1111/j.1475-4754.2012.00695.x.
Kassambara, A., Mundt, F., 2020. Factoextra: Extract and Visualize the Results of Multivariate Data Analyses.
Kendall, C., Eriksen, A.M.H., Kontopoulos, I., Collins, M.J., Turner-Walker, G., 2018. Diagenesis of archaeological bone and tooth. Palaeogeogr. Palaeoclimatol. Palaeoecol. 491, 21–37. https://doi.org/10.1016/j.palaeo.2017.11.041.
Kontopoulos, I., Penkman, K., Mullin, V.E., Winkelbach, L., Unterländer, M., Scheu, A., Kreutzer, S., Hansen, H.B., Margaryan, A., Teasdale, M.D., Gehlen, B., Street, M., Lynnerup, N., Liritzis, I., Sampson, A., Papageorgopoulou, C., Allentoft, M.E., Burger, J., Bradley, D.G., Collins, M.J., 2020. Screening archaeological bone for palaeogenetic and palaeoproteomic studies. PLoS One 15, 1–17. https://doi.org/10.1371/journal.pone.0235146.
Kontopoulos, I., Presslee, S., Penkman, K., Collins, M.J., 2018. Preparation of bone powder for FTIR-ATR analysis: the particle size effect. Vib. Spectrosc. 99, 167–177. https://doi.org/10.1016/j.vibspec.2018.09.004.
Koon, H.E.C., Nicholson, R.A., Collins, M.J., 2003. A practical approach to the identification of low temperature heated bone using TEM. J. Archaeol. Sci. 30, 1393–1399. https://doi.org/10.1016/S0305-4403(03)00034-7.
Koon, H.E.C., O'Connor, T.P., Collins, M.J., 2010. Sorting the butchered from the boiled. J. Archaeol. Sci. 37, 62–69. https://doi.org/10.1016/j.jas.2009.08.015.
Kuhn, M., Johnson, K., 2013. Applied Predictive Modeling. Springer-Verlag, New York.
Kuhn, M., Wing, J., Weston, S., Williams, A., Keefer, C., Engelhardt, A., Cooper, T., Mayer, Z., Kenkel, B., , Team, R Core, Benesty, M., Lescarbeau, R., Ziem, A., Scrucca, L., Tang, Y., Candan, C., Hunt, T., 2020. Caret: Classification and Regression Training.
Lantz, B., 2013. Machine Learning with R. Packt Publising, Birmingham.
Lê, S., Josse, J., Husson, F., 2008. FactoMineR: an R package for multivariate analysis. J. Stat. Software 25, 1–18.
Lebon, M., Reiche, I., Gallet, X., Bellot-Gurlet, L., Zazzo, A., 2016. Rapid quantification of bone collagen content by ATR-FTIR spectroscopy. Radiocarbon 58, 131–145. https://doi.org/10.1017/RDC.2015.11.
Lebon, M., Reiche, I., Bahain, J.J., Chadefaux, C., Moigne, A.M., Fröhlich, F., Sémah, F., Schwarcz, H.P., Falguères, C., 2010. New parameters for the characterization of diagenetic alterations and heat-induced changes of fossil bone mineral using Fourier transform infrared spectrometry. J. Archaeol. Sci. 37, 2265–2276. https://doi.org/10.1016/j.jas.2010.03.024.
Lebon, M., Reiche, I., Fröhlich, F., Bahain, J.J., Falguères, C., 2008. Characterization of archaeological burnt bones: contribution of a new analytical protocol based on derivative FTIR spectroscopy and curve fitting of the $\nu 1\nu 3$PO4domain. Anal. Bioanal. Chem. 392, 1479–1488. https://doi.org/10.1007/s00216-008-2469-y.
Lee-Thorp, J.A., van der Merwe, N.J., 1991. Aspects of the chemistry of modern and fossil biological apatites. J. Archaeol. Sci. 18, 343–354. https://doi.org/10.1016/0305-4403(91)90070-6.
Leskovar, T., Zupanič Pajnič, I., Geršak, Ž.M., Jerman, I., Črešnar, M., 2020. ATR-FTIR spectroscopy combined with data manipulation as a pre-screening method to assess DNA preservation in skeletal remains. Forensic Sci. Int. Genet. 44, 102196. https://doi.org/10.1016/j.fsigen.2019.102196.
Longin, R., 1971. New method of collagen extraction for radiocarbon dating. Nature 230, 241–242. https://doi.org/10.1038/230241a0.
Macphail, R.I., Courty, M.-A., Hather, J., Wattez, J., Ryder, M., Cameron, N., Branch, N. P., 1997. The soil micromorphological evidence of domestic occupation and stabling activities. In: Maggi, R. (Ed.), Arene Candide: A Functional and Environmental Assessment of the Holocene Sequence(Excavations Bernarbo' Brea-Cardini 1940–50). Il Calamo, Roma, pp. 53–88.
Madupalli, H., Pavan, B., Tecklenburg, M.M.J., 2017. Carbonate substitution in the mineral component of bone: discriminating the structural changes, simultaneously imposed by carbonate in A and B sites of apatite. J. Solid State Chem. 255, 27–35. https://doi.org/10.1016/j.jssc.2017.07.025.
Marginedas, F., Rodríguez-Hidalgo, A., Soto, M., Bello, S.M., Cáceres, I., Huguet, R., Saladié, P., 2020. Making skull cups: butchering traces on cannibalised human skulls from five European archaeological sites. J. Archaeol. Sci. 114 https://doi.org/10.1016/j.jas.2020.105076.
Marques, M.P.M., Mamede, A.P., Vassalo, A.R., Makhoul, C., Cunha, E., Gonçalves, D., Parker, S.F., Batista de Carvalho, L.A.E., 2018. Heat-induced bone diagenesis probed by vibrational spectroscopy. Sci. Rep. 8, 1–13. https://doi.org/10.1038/s41598-018-34376-w.
Martín-Rodríguez, P., 2015. Caracterización Zooarqueológica De Las Cuevas Redil En La Prehistoria De La Meseta Norte: El Caso De El Mirador (Sierra De Atapuerca, Burgos). Dr. Diss. Univ. Rovira i Virgili.
Martín-Rodríguez, P., Vergès, J.M., 2016. Bone alterations in fumiers: experimental approach. Quat. Int. 414, 294–303. https://doi.org/10.1016/j.quaint.2015.12.056.
Martín, P., Tornero, C., García, D.C.S., Vergès, J.M., 2021. Early sheep herd management in the inland of the Iberian Peninsula: results of the incremental isotopic analyses of dental remains from El Mirador cave (Sierra de Atapuerca, Spain). Archaeol Anthropol Sci 13, 99. https://doi.org/10.1007/s12520-021-01355-8.
Miller, N., 1996. Seed eaters of the ancient near east: human or herbivore? Curr. Anthropol. 37, 521–528.
Moclán, A., Domínguez-Rodrigo, M., Yravedra, J., 2019. Classifying agency in bone breakage: an experimental analysis of fracture planes to differentiate between hominin and carnivore dynamic and static loading using machine learning (ML) algorithms. Archaeol. Anthropol. Sci. 11, 4663–4680. https://doi.org/10.1007/s12520-019-00815-6.
Moclán, A., Huguet, R., Márquez, B., Laplana, C., Arsuaga, J.L., Pérez-González, A., Baquedano, E., 2020. Identifying the bone-breaker at the Navalmaíllo Rock Shelter (Pinilla del Valle, Madrid) using machine learning algorithms. Archaeol. Anthropol. Sci. 12 https://doi.org/10.1007/s12520-020-01017-1.
Munro, L.E., Longstaffe, F.J., White, C.D., 2007. Burning and boiling of modern deer bone : effects on crystallinity and oxygen isotope composition of bioapatite phosphate. Paleogeography, Paleoclimatology, Paleoecol. 249, 90–102. https://doi.org/10.1016/j.palaeo.2007.01.011.
Nicholson, R.A., 1998. Bone degradation in a compost heap. J. Archaeol. Sci. 25, 393–403. https://doi.org/10.1006/jasc.1997.0208.
Nicholson, R.A., 1996. Bone degradation, burial medium and species representation: debunking the myths, an experiment-based approach. J. Archaeol. Sci. 23, 513–533. https://doi.org/10.1006/jasc.1996.0049.
Nielsen-Marsh, C.M., Hedges, R.E.M., 2000. Patterns of diagenesis in bone I: the effects of site environments. J. Archaeol. Sci. 27, 1139–1150. https://doi.org/10.1006/jasc.1999.0537.
Oms, F.X., López-García, J.M., Mangado, X., Martín, P., Mendiela, S., Morales, J.I., Pedro, M., Rodríguez, A., Rodríguez-Cintas, A., Yubero, M., 2013. Hàbitat en cova i espai pels ramats ca. 6200-6000 BP: La Cova Colomera (Prepirineu de Lleida) durant el Neolític antic. Saguntum (P.L.A.V.) 45, 25–38.
Opitz, D., Maclin, R., 1999. Popular ensemble methods: an empirical study. J. Artif. Intell. Res. 11, 169–198. https://doi.org/10.1613/jair.614.
Paschalis, E.P., Mendelsohn, R., Boskey, A.L., 2011. Infrared assessment of bone quality: a review. Clin. Orthop. Relat. Res. 469, 2170–2178. https://doi.org/10.1007/s11999-010-1751-4.
Pasteris, J.D., Wopenka, B., Valsami-Jones, E., 2008. Bone and tooth mineralization: why apatite? Elements 4, 97–104. https://doi.org/10.2113/Gselements.4.2.97.
Pasteris, J.D., Yoder, C.H., Wopenka, B., 2014. Minerals in the human body: molecular water in nominally unhydrated carbonated hydroxylapatite: the key to a better understanding of bone mineral. Am. Mineral. 99, 16–27. https://doi.org/10.2138/am.2014.4627.
Polo-Díaz, A., Benito-Calvo, A., Martínez-Moreno, J., Mora Torcal, R., 2016. formation processes and stratigraphic integrity of the middle-to-upper palaeolithic sequence at cova gran de Santa linya (southeastern prepyrenees of lleida, iberian peninsula). Quat. Int. 417, 16–38. https://doi.org/10.1016/j.quaint.2015.10.113.
Polo-Díaz, A., 2010. Rediles prehistóricos y uso del espacio en abrigos bajo roca en la Cuenca Alta del Ebro: geoarqueología y procesos de formación durante el Holoceno. Universidad del País Vasco-Euskal Herriko Unibertsitatea (UPV-EHU).
Pijoan, C.M., Mansilla, J., Leboreiro, I., Lara, V.H., Bosch, P., 2007. Thermal alterations in archaeological bones. Archaeometry 49, 713–727. https://doi.org/10.1111/j.1475-4754.2007.00331.x.
R Core Team, 2017. R: A Language and Environment for Statistical Computing. R Foundation for Statistical Computing, Vienna, Austria. https://www.R-project.org/.
Roberts, S.J., Smith, C.I., Millard, A., Collins, M.J., 2002. The Taphonomy of cooked bone: characterizing boiling and its physuco-chemical effects. Archaeometry 44, 485–494.
Rodríguez, A., Allué, E., Buxó, R., 2016. Agriculture and livestock economy among prehistoric herders based on plant macro-remains from El Mirador (Atapuerca, Burgos). Quat. Int. 414, 272–284. https://doi.org/10.1016/j.quaint.2016.01.045.
Rokach, L., 2010. Ensemble-based classifiers. Artif. Intell. Rev. 33, 1–39. https://doi.org/10.1007/s10462-009-9124-7.
Sagi, O., Rokach, L., 2018. Ensemble learning: a survey. Wiley Interdiscip. Rev. Data Min. Knowl. Discov. 8, 1–18. https://doi.org/10.1002/widm.1249.
Shahack-Gross, R., 2011. Herbivorous livestock dung: formation, taphonomy, methods for identification, and archaeological significance. J. Archaeol. Sci. 38, 205–218. https://doi.org/10.1016/j.jas.2010.09.019.
Shahack-Gross, R., Albert, R.M., Gilboa, A., Nagar-Hilman, O., Sharon, I., Weiner, S., 2005. Geoarchaeology in an urban context: the uses of space in a Phoenician monumental building at Tel Dor (Israel). J. Archaeol. Sci. 32, 1417–1431. https://doi.org/10.1016/j.jas.2005.04.001.
Shahack-Gross, R., Marshall, F., Weiner, S., 2003. Geo-ethnoarchaeology of pastoral sites: the identification of livestock enclosures in abandoned Maasai settlements. J. Archaeol. Sci. 30, 439–459. https://doi.org/10.1006/jasc.2002.0853.
Shemesh, A., 1990. Crystallinity and diagenesis of sedimentary apatites. Geochem. Cosmochim. Acta 54, 2433–2438. https://doi.org/10.1016/0016-7037(90)90230-I.
Shipman, P., Fosterb, G., Schoeninger, M., 1984. Burnt Bones and Teeth : an Experimental Study of Color , Morphology , Crystal Structure and Shrinkage.
Snoeck, C., Lee-Thorp, J.A., Schulting, R.J., 2014. From bone to ash: compositional and structural changes in burned modern and archaeological bone. Palaeogeogr. Palaeoclimatol. Palaeoecol. 416, 55–68. https://doi.org/10.1016/j.palaeo.2014.08.002.
Spengler, R.N., 2019. Dung burning in the archaeobotanical record of West Asia: where are we now? Veg. Hist. Archaeobotany 28, 215–227. https://doi.org/10.1007/s00334-018-0669-8.
Sponheimer, M., Lee-Thorp, J.A., 1999. Alteration of enamel carbonate environments during fossilization. J. Archaeol. Sci. 26, 143–150. https://doi.org/10.1006/jasc.1998.0293.
Sponheimer, M., Ryder, C.M., Fewlass, H., Smith, E.K., Pestle, W.J., Talamo, S., 2019. Saving Old Bones: a non-destructive method for bone collagen prescreening. Sci. Rep. 9, 1–7. https://doi.org/10.1038/s41598-019-50443-2.

Stiner, M.C., Kuhn, S.L., Weiner, S., 1995. Differential burning, recrystallization, and fragmentation of archaeological bone. J. Archaeol. Sci. 22, 223–237.
Thompson, T.J.U., Gauthier, M., Islam, M., 2009. The application of a new method of Fourier Transform Infrared Spectroscopy to the analysis of burned bone. J. Archaeol. Sci. 36, 910–914. https://doi.org/10.1016/j.jas.2008.11.013.
Thompson, T.J.U., Islam, M., Bonniere, M., 2013. A new statistical approach for determining the crystallinity of heat-altered bone mineral from FTIR spectra. J. Archaeol. Sci. 40, 416–422. https://doi.org/10.1016/j.jas.2012.07.008.
Trueman, C.N., Palmer, M.R., Field, J., Privat, K., Ludgate, N., Chavagnac, V., Eberth, D. A., Cifelli, R., Rogers, R.R., 2008. Comparing rates of recrystallisation and the potential for preservation of biomolecules from the distribution of trace elements in fossil bones. Comptes Rendus Palevol 7, 145–158.
Trueman, C.N.G., Behrensmeyer, A.K., Tuross, N., Weiner, S., 2004. Mineralogical and compositional changes in bones exposed on soil surfaces in Amboseli National Park, Kenya: diagenetic mechanisms and the role of sediment pore fluids. J. Archaeol. Sci. 31, 721–739. https://doi.org/10.1016/j.jas.2003.11.003.
Venables, W.N., Ripley, B.D., 2002. Modern Applied Statistics with S.
Vergès, J.M., Allué, E., Fontanals, M., Morales, J.I., Martín, P., Carrancho, Á., Expósito, I., Guardiola, M., Lozano, M., Marsal, R., Oms, X., Euba, I., Rodríguez, A., 2016. El mirador cave (Sierra de Atapuerca, burgos, Spain): a whole perspective. Quat. Int. 414, 236–243. https://doi.org/10.1016/j.quaint.2016.01.044.
Weiner, S., 2010. Microarchaeology: beyond the Visible Archaeological Record. Cambridge University Press. https://doi.org/10.1017/CBO9780511811210.
Weiner, S., Wagner, H.D., 1998. Thematerial bone: structure mechanical function relations. Annu. Rev. Mater. Sci. 28, 271–298.
Weiner, S., Bar-Yosef, O., 1990. States of preservation of bones from prehistoric sites in the Near East: a survey. J. Archaeol. Sci. 17, 187–196. https://doi.org/10.1016/0305-4403(90)90058-D.
White, T.D., 1992. Prehistoric Cannibalism at Mancos 5MTUMR-2346. Princeton University Press, Princeton, NJ.
Wright, L.E., Schwarcz, H.P., 1996. Infrared and isotopic evidence for diagenesis of bone apatite at dos pilas, Guatemala: palaeodietary implications. J. Archaeol. Sci. 23, 933–944. https://doi.org/10.1006/jasc.1996.0087.